JOURNAL OF SOLID STATE CHEMISTRY 96, 271–286 (1992)

Thallium Nonstoichiometry in 2212-Thallium Cuprate

C. MICHEL, C. MARTIN,[1] M. HERVIEU, A. MAIGNAN, J. PROVOST, M. HUVE, AND B. RAVEAU

Laboratoire CRISMAT, ISMRa, Bd du Maréchal Juin, 14050 Caen Cedex, France

Received March 11, 1991; in revised form July 5, 1991

The study of thallium nonstoichiometry in the thallium 2212 cuprate by X-ray diffraction and electron microscopy has allowed a significant homogeneity range to be isolated. $Tl_{2-x}Ba_2CaCu_2O_{8\pm\delta}$ with $0 \leq x < 0.4$. The HREM study showed that thallium deficiency is not accomodated through an intergrowth mechanism but implies a statistical distribution of Tl atoms and vacancies in the thallium double layers. However, it appeared that modulated areas can arise from ions' and vacancies' local orderings in the (111) plane of the rock salt layers; they result in satellites in the E.D. patterns. The study of the superconducting properties of these oxides shows that the critical temperature is not greatly affected by the thallium nonstoichiometry, whereas hydrogen–argon annealings confirm the predominant role of oxygen non stoichiometry upon T_c's, allowing a $(T_c)_{R=0}$ of 120 K to be reached for $x = 0.4$. The deterioration of the grain boundaries by hydrogen annealing is also studied.

Introduction

The numerous studies of the superconducting properties of the 2212-thallium cuprate have shown that the critical temperature of this phase can vary in a significant way, according to the authors, from 96 to about 108 K (*1–7*). This apparent divergence between the different results is explained by the variations of oxygen stoichiometry according to the experimental conditions of synthesis (*8–13*). Recent studies (*14–17*) have shown that the critical temperature of thallium cuprates can be increased several degrees and even several tens of degrees by hydrogen annealing at low temperature. However, oxygen is not the only factor which can influence the hole carrier density in this oxide. Thallium is susceptible to migration in the structure, from the rock salt-type layers toward the calcium sites, as shown from several structural studies (*1, 18–20*). Consequently, it appears most likely that the stoichiometric composition $Tl_2Ba_2CaCu_2O_8$ is not the only possible representative formula of the 2212 superconductor. We report here on the relationships between thallium nonstoichiometry in this oxide and its structural and superconducting properties.

Experimental

Samples were prepared from mixtures of Tl_2O_3, BaO_2, CaO, and CuO in adequate molar ratios in order to obtain the nominal compositions $Tl_{2-x}Ba_2CaCu_2O_{10-(3x/2)}$. The powders were pressed in bars and heated in sealed quartz tubes at 890°C for 8 hr. The

[1] To whom correspondence should be addressed.

0022-4596/92 $3.00

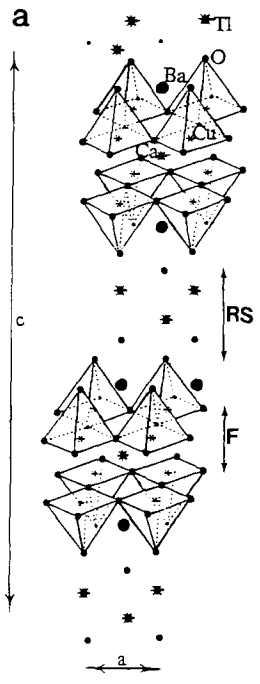

FIG. 1a. Idealized drawing of the 2212-type structure.

weight of starting material was calculated so as to reach an oxygen pressure of about 10 bars, admitting that BaO_2 decomposes into BaO and molecular oxygen during reaction, and taking into consideration the approximate dimensions of the tube.

The powder X-ray diffraction patterns were registered by step scanning over an angular range of $10° \leq 2\theta \leq 120°$ in increments of 0.02° by means of a Philips diffractometer using the Cu $K\alpha$ radiation. The Bragg reflections were used to refine the cell parameters and the crystal structure with the profile refinement computer program DBW 3.2 (*21*). Scattering factors for ions were used.

The electron diffraction study was performed with a JEOL 120 CX electron microscope fitted with a side entry goniometer ($\pm 60°$) and the high resolution electron microscopy (HREM) with a JEM 200 CX microscope fitted with a top entry goniometer ($\pm 10°$) and an objective lens with c_s = 0.8 mm.

The superconducting properties were studied by ac susceptibility and ac resistivity measurements at temperatures down to

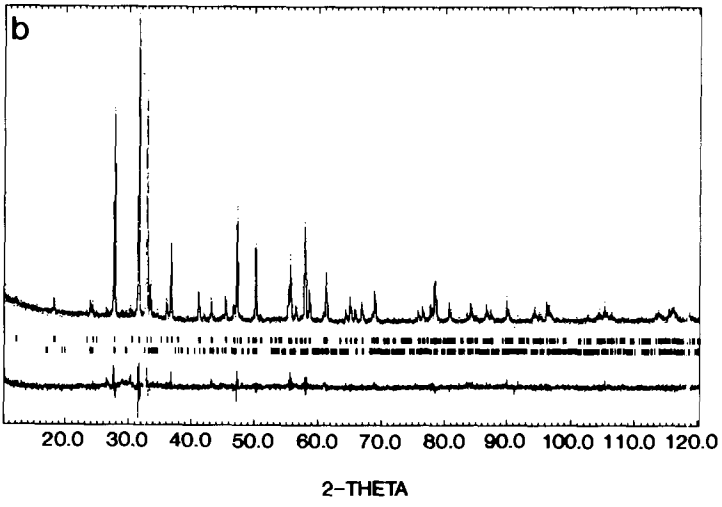

FIG. 1b. Experimental, calculated, and difference powder X-ray diffraction patterns for the $Tl_{1.6}$ sample with $BaCO_3$ as impurity.

TABLE I

REFINED PARAMETERS AND STANDARD DEVIATIONS FOR $Tl_2Ba_2CaCu_2O_{8\pm\delta}$ AND $Tl_{1.6}Ba_2CaCu_2O_{8\pm\delta}$

Atoms	Parameters	$Tl_2Ba_2CaCu_2O_{8\pm\delta}$	$Tl_{1.6}Ba_2CaCu_2O_{8\pm\delta}$
Tl	Tl/Ca	3.66/0.34(2)	3.44/0.18(2)
4*e*(1/4, 1/2, *z*)	*z*	0.2134(1)	0.2132(1)
	B(Å^2)	1.02(6)	0.50(5)
Ba	*z*	0.1216(1)	0.1213(1)
4*e*(0, 0, *z*)	B(Å^2)	0.03(7)	0.53(6)
Ca	Ca/Tl	1.66/0.34(2)	1.82/0.18(2)
2*a*(0, 0, 0)	B(Å^2)	0.5(3)	0.3(2)
Cu	*z*	0.0535(2)	0.0545(2)
4*e*(1/2, 1/2, *z*)	B(Å^2)	0.1(4)	0.2(1)
O(1)	*z*	0.0508(6)	0.0510(6)
8*g*(0, 1/2, *z*)	B(Å^2)	1.0	1.0
O(2)	*z*	0.1428(10)	0.1461(8)
4*e*(1/2, 1/2, *z*)	B(Å^2)	1.0	1.0
O(3)	*z*	0.2793(10)	0.2838(9)
4*e*(1/2, 1/2, *z*)	B(Å^2)	1.0	1.0
	a(Å)	3.8565(1)	3.8489(1)
	c(Å^2)	29.3122(9)	29.3153(7)
	R_p(%)	8.21	7.24
	R_{wp}(%)	10.67	9.40
	R_{exp}(%)	9.85	9.79
	R_i(%)	7.81	7.23

4.2 K. No demagnetization corrections were made.

Results and Discussion

The X-ray diffraction analysis of the final products suggests that the 2212-type structure is pure for $0 \leq x < 0.40$, leading to the formula $Tl_{2-x}Ba_2CaCu_2O_{8\pm\delta}$. For the limit composition $x = 0.4$, some extra weak diffraction peaks were observed, some of them indicating the presence of $BaCO_3$.

Thallium Deficiency

In order to check the possibility of thallium deficiency in the 2212 structure, structural refinements were performed on the two limits $Tl_2Ba_2CaCu_2O_{8\pm\delta}$ and $Tl_{1.6}Ba_2CaCuO_{8\pm\delta}$, taking especially into consideration the occupancy factors of the cationic sites, i.e., Tl and Ca sites.

From the previous crystal structure determinations of the oxide $Tl_2Ba_2CaCu_2O_8$ (*1*, *19*, *20*) it is well known that the structure of this oxide consists of double pyramidal copper layers intergrown with triple rock salt layers involving thallium bilayers. The previous works on single crystals and powders have also shown, for this nominal composition, the possibility of cation exchanges between thallium and calcium layers. In the present work, $Tl_2Ba_2CaCu_2O_{8\pm\delta}$ was used as a reference assuming that crystallographic sites were fully occupied.

TABLE II

CALCULATED INTERATOMIC DISTANCES (IN Å) FOR $Tl_{1.6}Ba_2CaCu_2O_{8\pm\delta}$

M–O	*d*	*M*–O	*d*
Tl–O(2)	1.96(3) × 1	Ba–O(3)	2.78(3) × 1
Tl–O(3)	2.08(3) × 1		
Tl–O(3)	2.723(1) × 4	Ca–O(1)	2.44(2) × 8
Ba–O(1)	2.82(1) × 4	Cu–O(1)	1.926 × 4
Ba–O(2)	2.82(1) × 4	Cu–O(2)	2.68(3) × 1

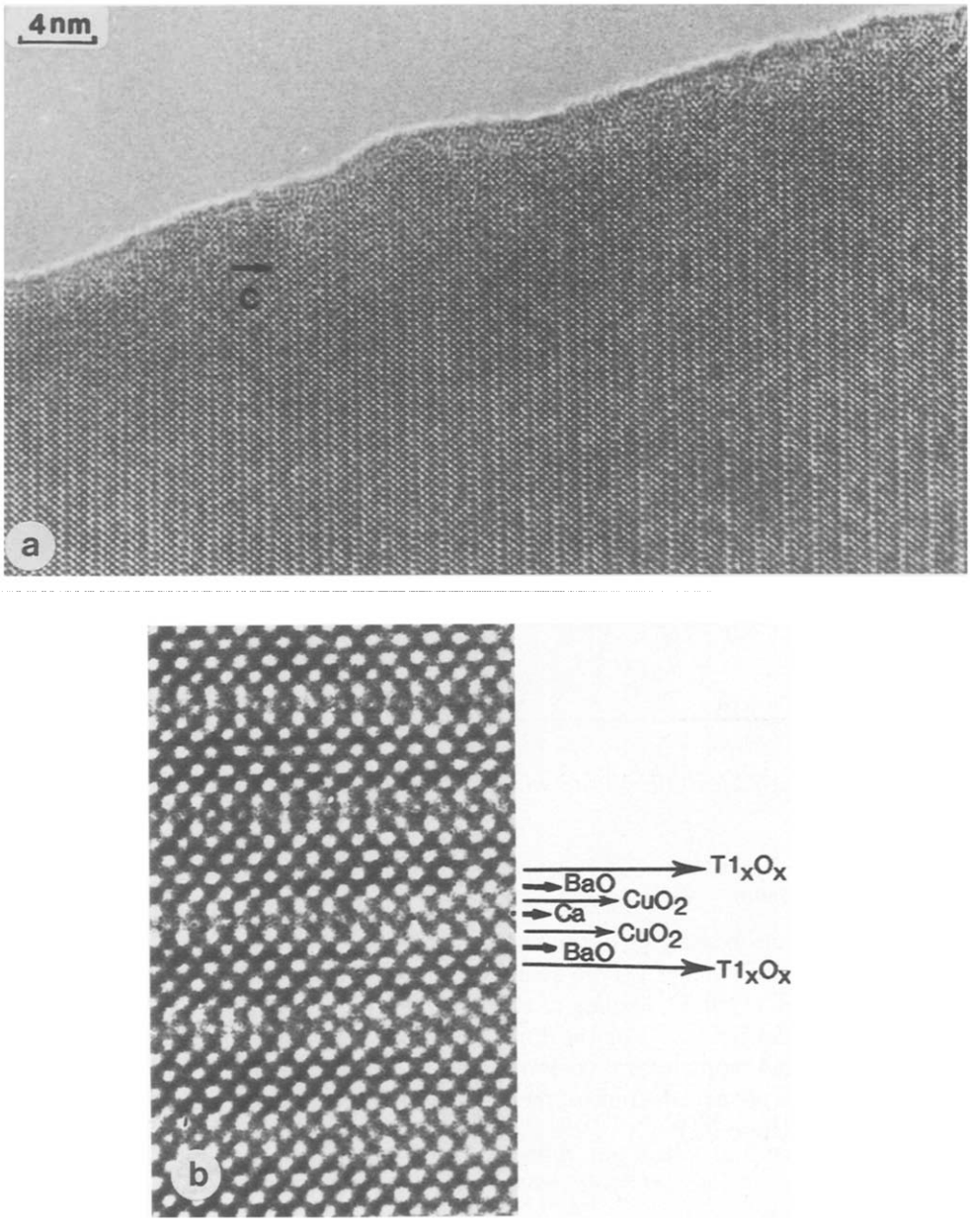

FIG. 2. [100] HREM images of the thallium deficient phase: (a) a high evenness of the contrast is observed in most of the crystals; (b) enlargement of an image (focus value $\Delta f \approx -700$ Å) showing the correlation between the rows of white dots and the atomic layers.

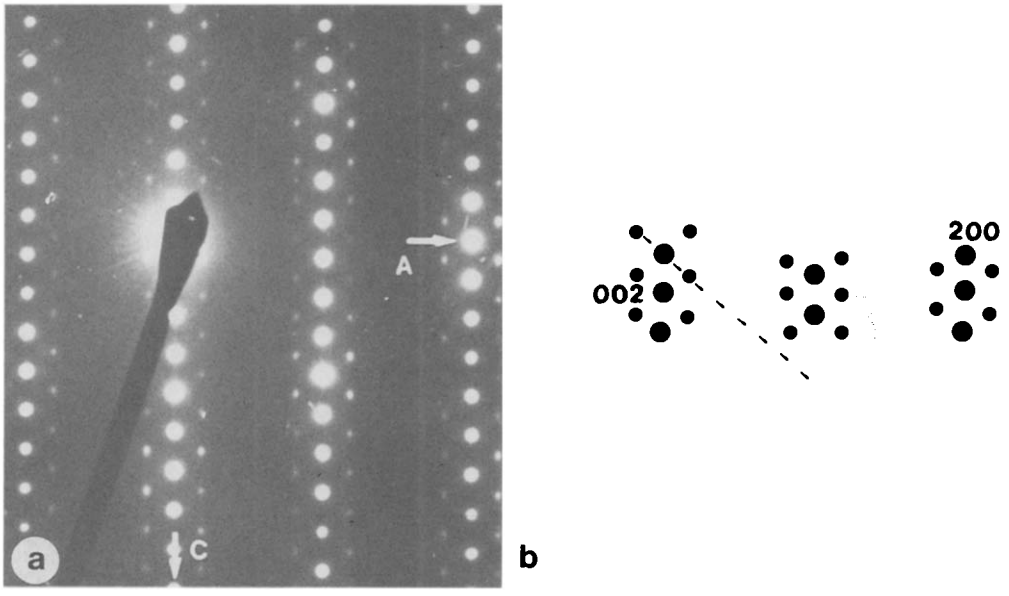

FIG. 3. (a) [010] electron diffraction pattern showing weak satellites (along [106]*); (b) schematic drawing.

Successive refinements of the positional parameters, of the ratio Tl/Ca, and of the isotropic thermal factors for cations allowed the R factors to be lowered to $R_p = 8.21\%$, $R_{wp} = 10.67\%$ ($R_{exp} = 9.85\%$), $R_i = 7.81\%$, where R_p, R_{wp}, and R_i are the agreement factors for profile, weighted profile, and intensity, respectively. The values of the different variables are given in Table I. Our results confirm the presence of thallium on calcium sites with an amount of 17%, close to that observed by single crystal studies, i.e., ranging from 10% (*20*) to 15–28% (*19*). Concerning the thallium sites, our refinements lead to the "presence" of 73 electrons instead of 78 electrons if they were fully occupied by thallium. This occupancy of thallium sites is also very close to that observed by Subramanian *et al.* (*20*) and Morosin *et al.* (*19*) who obtained 72 and 68–73 electrons, respectively. Thus, for these experimental conditions of synthesis, the reference compound $Tl_2Ba_2CaCu_2O_8$ has not lost thallium, since it can be formulated $[Tl_{1.83}Ca_{0.17}]_{RS}Ba_2[Ca_{0.83}Tl_{0.17}]_FCu_2O_{8\pm\delta}$ (RS for rock salt layers and F for the $[Ca]_\infty$ fluorite-type layers located between the two $[CuO_2]_\infty$ pyramidal layers, Fig. 1a).

For the thallium deficient nominal composition $Tl_{1.6}Ba_2CaCu_2O_{9.4}$, the refined parameters obtained for the stoichiometric 2212 phase were used in a first step. As stated before, some extra diffraction peaks were observed in the diffraction pattern, some of them corresponding to $BaCO_3$, which is the main impurity. The highest peak of $BaCO_3$ represented 4% in intensity of the highest peak of the 2212 phase. The other extra peaks, mainly at 26.5°, 28.9°, and 30.3° (in 2θ) appeared at a lower level and were not attributed. For these reasons, only $BaCO_3$ was introduced in the calculations as a secondary phase. After refinement of the peak shape, the following R factors were obtained: $R_p = 7.37\%$, $R_{wp} = 9.56\%$, and $R_i = 8.50\%$. At this stage, thallium deficiency was assumed. Starting from a full occupancy of the different cationic sites,

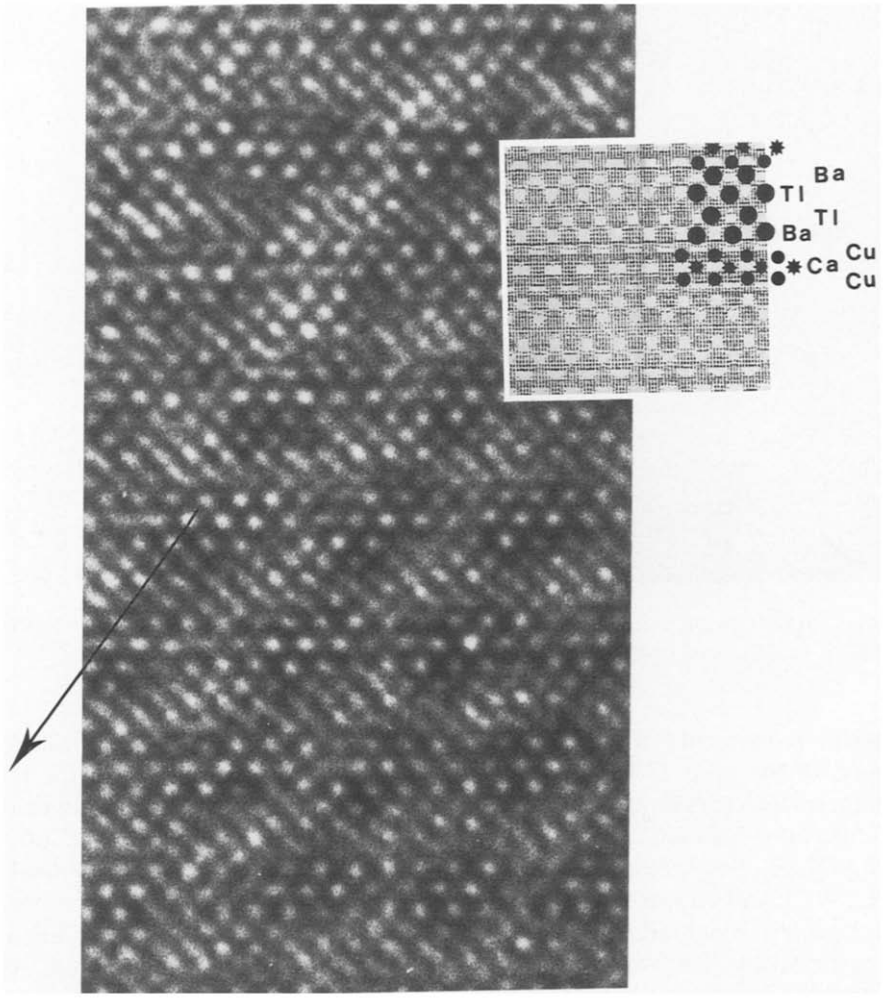

FIG. 4. HREM [010] image of a tiny part of a crystal, showing modulations of the contrast. The focus value is close to -400 Å ($\approx$ Scherzer value). The corresponding calculated image is inserted and the cations positions are represented.

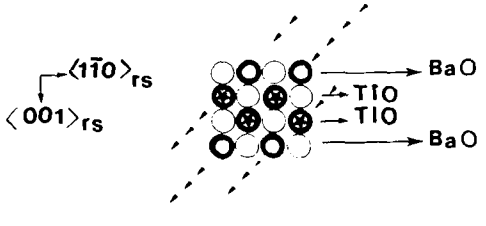

FIG. 5. Idealized drawing of the triple rock salt slice built up from four AO layers, $\langle 110\rangle_{RS}$ corresponds to $\langle 100\rangle_P$, i.e., $\langle 100\rangle$ of the 2212 structure.

successive refinements on occupancy factors of those sites and of positional parameters led to the R factors $R_p = 7.24\%$, $R_{wp} = 9.40\%$, and $R_j = 7.23\%$, for the atomic coordinates given in Table I. Experimental, calculated, and difference patterns are plotted in Fig. 1b. The most important result of these calculations deals with the fact that one observes a significant thallium deficiency in the rock salt layers, since one obtains 68 electrons on these sites, which corresponds to the lowest value obtained by

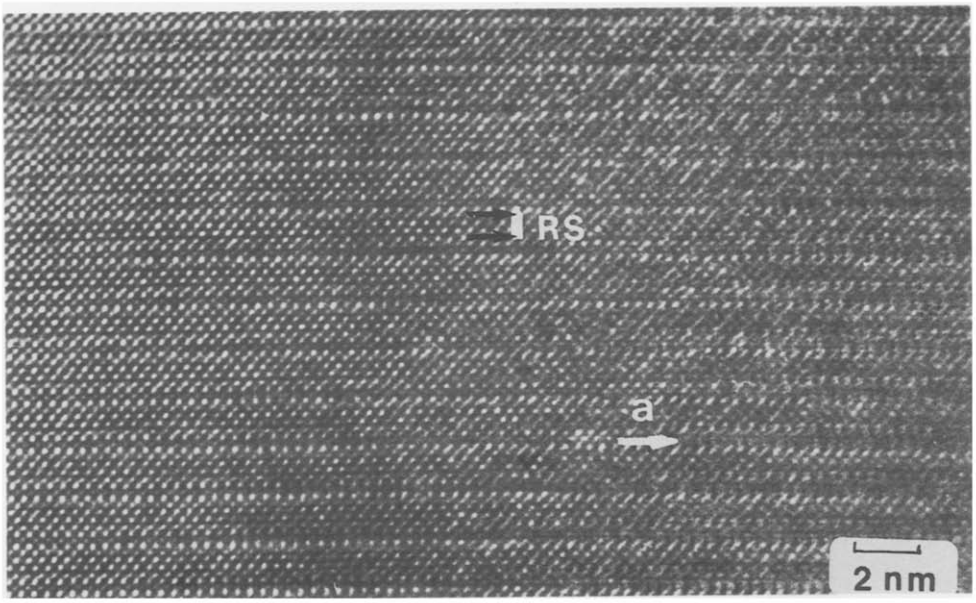

FIG. 6. Other example of contrast variations in $(111)_{RS}$ planes. A modulation with $q = 2 \times d_{100}$ is observed in the right part of the image. The four AO layers of the rock salt slice are outlined (white).

Morosin *et al.* (*19*) from single crystal refinements. One also observes the presence of thallium in the calcium sites; however, the amount of thallium on the latter sites (9%) is much smaller than in the limit $Tl_2Ba_2CaCu_2O_{8\pm\delta}$ (17%). Moreover, it is worth pointing out that the thallium content deduced from the structural study is higher than that expected from the nominal composition, in agreement with the presence of impurities. Thus the limit thallium deficient phase can be formulated $[Tl_{1.72}Ca_{0.09}]_{RS}Ba_2[Ca_{0.91}Tl_{0.09}]_FCu_2O_{8\pm\delta}$.

Note that the "O_8" composition was attributed to both compounds in the calculations, in spite of the possible existence of oxygen nonstoichiometry, owing to the fact that several attempts to refine oxygen occupancy did not allow significant variation of the R factor to be detected.

Electron Microscopy

The two extreme nominal compositions $x = 0$ and $x = 0.4$ were chosen for electron microscopy study. The systematic observation and recording of numerous [100] and [110] electron diffraction patterns showed for both oxides the absence of extra spots or diffuse streaks along **c**; this attests to the high regularity of the layer stacking according to a 2212-type sequence, in agreement with the corresponding lattice images. Moreover, the HREM observations show a high evenness of the contrast at the level of the AO layers in most of the crystals and throughout large areas of the crystals (Fig. 2a). This feature attests, for the thallium deficient oxide, to the statistical distribution of thallium cations and vacancies in the rock salt layers. The experimental through focus series give evidence of similar images in both stoichiometric and thallium deficient oxides, in agreement with the small differences of the scattering factors in the [AO] layers. Figure 2b shows an example where a direct analysis of the atomic planes allows the white dots to be correlated with cations positions for focus values close to -700 Å.

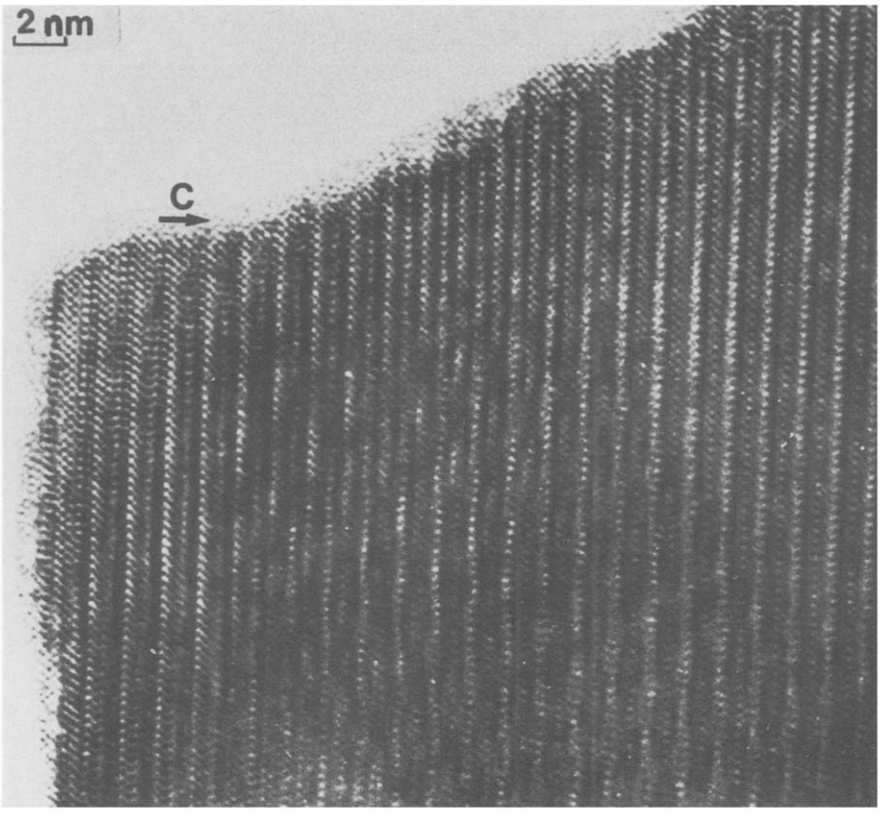

FIG. 7. [100] image of a crystal showing strong undulations of the atomic layers; the amplitude of the phenomenon is similar to that of the bismuth oxides but the direction and the frequency are different.

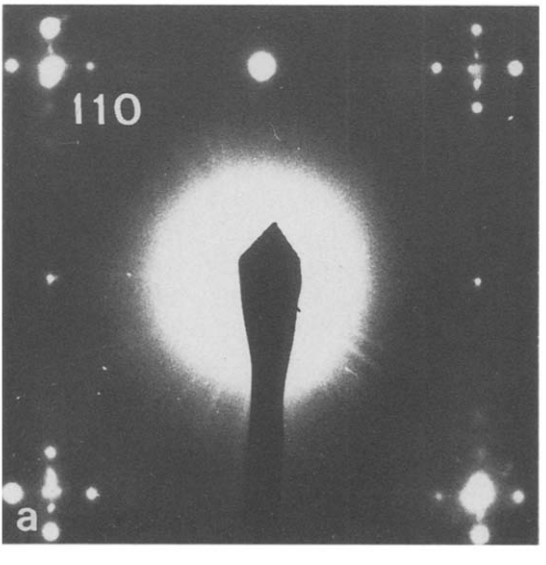

FIG. 8. (a) [001] electron diffraction pattern exhibiting satellites along [100]* and [010]*; (b) [001] image showing a modulation of the contrast established along **a**. In that part of the crystal, the periodicity is close to six times d_{100}; (c) [001] image showing a bidimensional modulation.

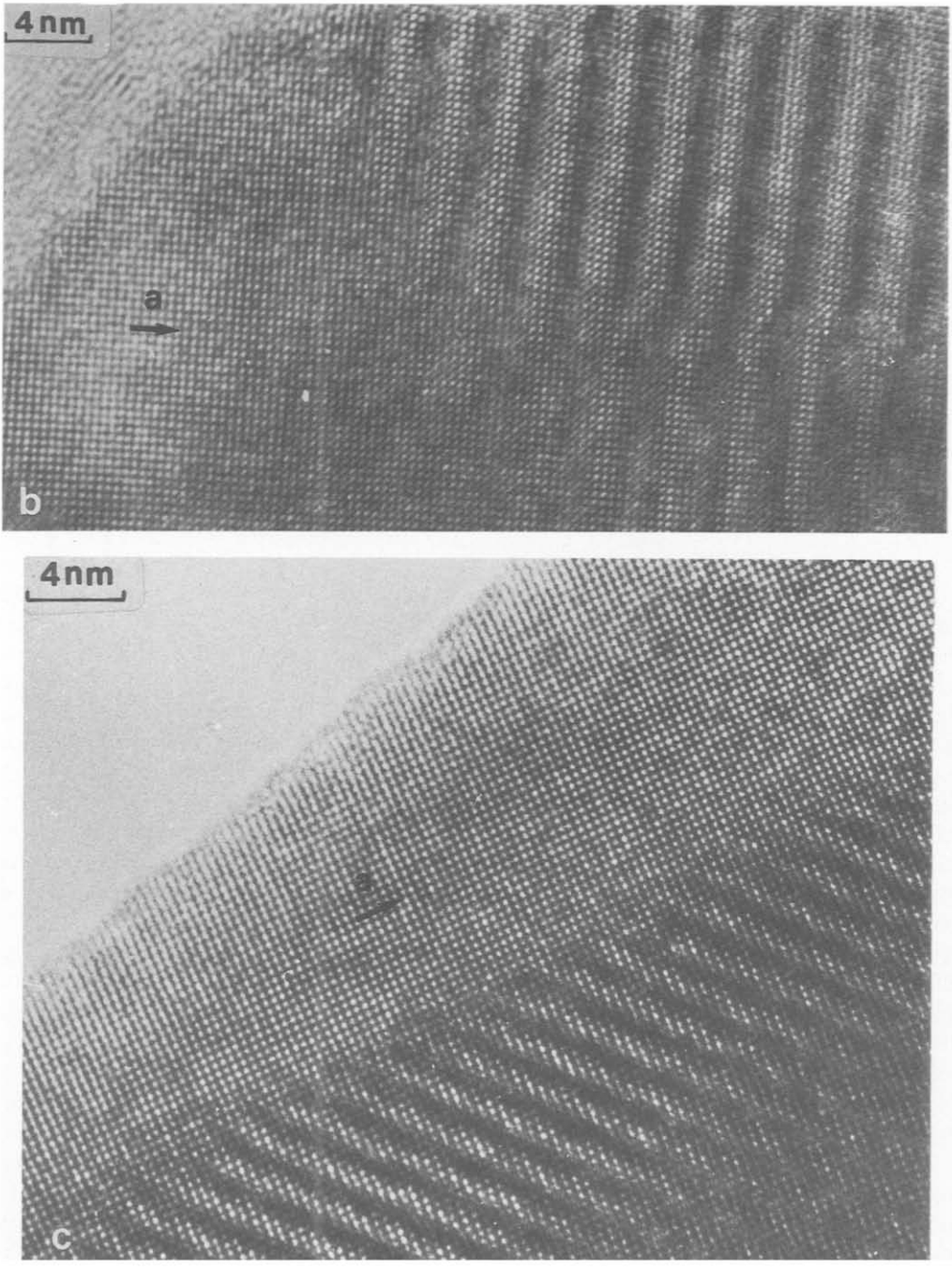

FIG. 8—*Continued*

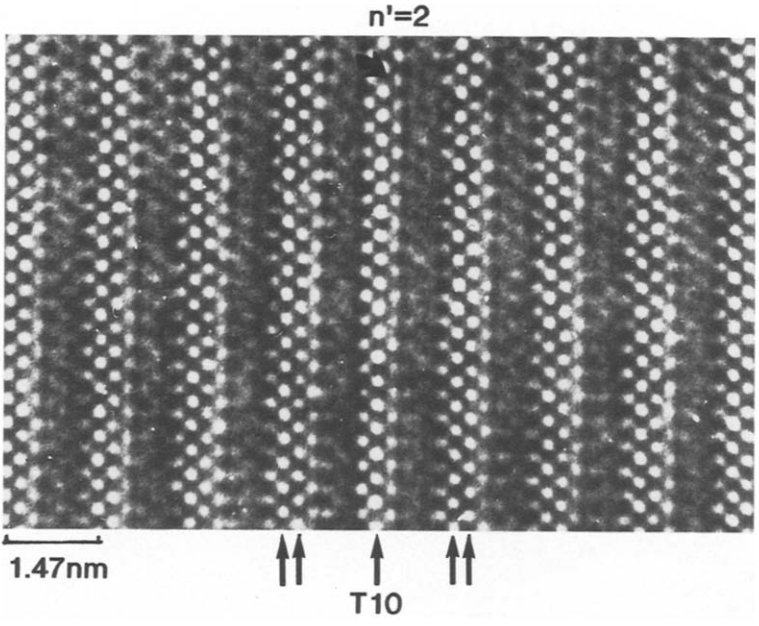

FIG. 9. $n' = 2$ defective slice in an $n = 3$ matrix. The $[TIO]_x$ layers are black arrowed.

Structure modulation. The main difference between the stoichiometric and the thallium-deficient phase deals with the existence of modulations of the structure. In the stoichiometric phase, one observes very rarely satellites in the E.D. patterns. To the contrary, weak satellites are frequently observed in the [100] E.D. patterns of the thallium-deficient oxide. The incommensurate modulation with respect to the basic lattice is shown in Fig. 3; satellites lie along [106]*, and the wavelength of the modulation along A is close to 5.4 times the d_{100} distance. This difference between the stoichiometric and thallium-deficient samples may explain the disagreement between the different authors about the existence of modulations which appeared at the beginning of the study of thallium cuprates (*23, 25*).

The incommensurate satellites are systematically associated with the existence of more or less extended areas where the contrast is modulated. This suggests that the intensity of the satellites, which varies from one crystal to the other, is directly correlated to the extent of the modulated zone. Through focus series have been recorded for tiny modulated areas located on crystal edges. The interpretation of the contrast of such images does not allow a reliable model to be proposed, since the contrast variations can be correlated either to changes of the ion nature (and vacancies) or to ion displacements or to both simultaneously. However, some important information can be obtained:

(i) The direction of the modulations is in agreement with the position of the satellites in the E.D. patterns and, in the same way, the wavelength along the **a** axis is consistent.

(ii) Images where cations are highlighted showed that thallium and barium atoms in $[AO]_x$ layers are mainly hit by the variations of contrast, whereas $[Ca]_x$ appear as the less disturbed. Images where the low electronic density zones are brightest showed that the oxygen sites are also involved in the modu-

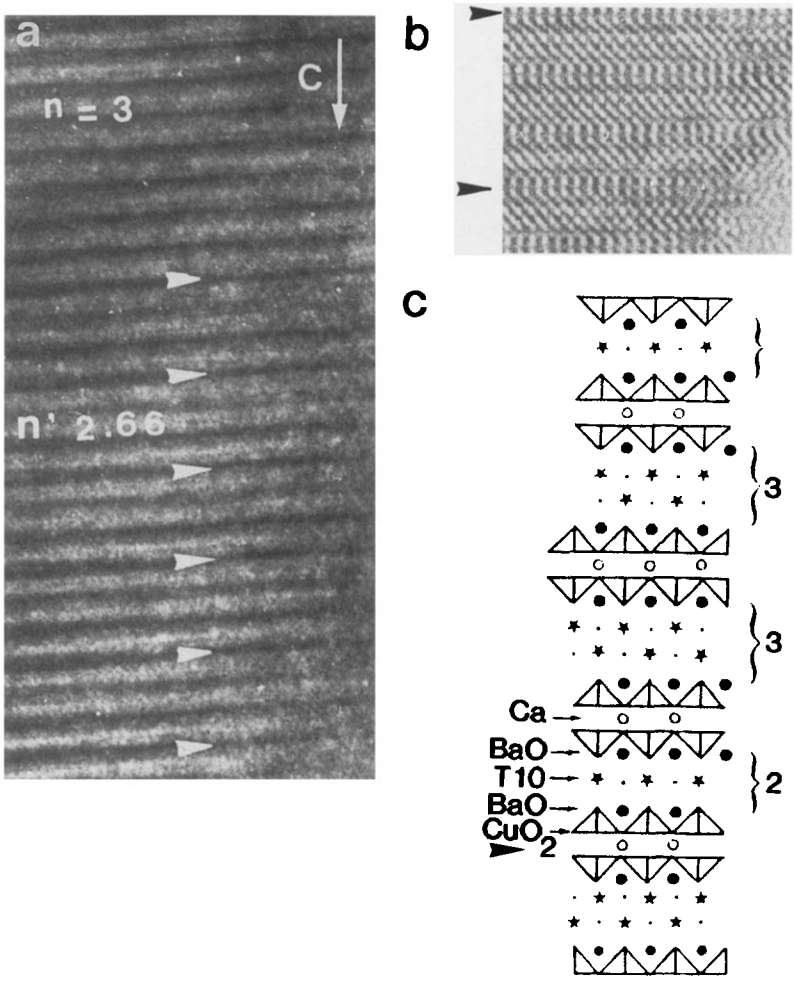

FIG. 10. $n' = 2.66$: (a) image of a part of a crystal where an $n' = 2.66$ member is observed. It corresponds to the regular sequence [$n = 3$, $n = 3$, $n = 2$]; (b) high resolution image of a crystal edge of one member 2.66; (c) idealized drawing of the intergrowth $n' = 2.66$.

lation; an example is shown in Fig. 4. In that [010] image, recorded for a focus value close to -400 Å (close to Scherzer value), the white dots are correlated to oxygen atoms and oxygen vacancies; the image calculated for a nonmodulated zone (same focus value) is inserted for comparison, and the positions of cations are drawn as black dots and stars. It appears clearly that the modulation of contrast hit also the anions (and vacancies) sites. Moreover from these images, variations of the positions of the ions are also observable, leading to slightly wavy rock salt layers.

These observations suggest that the modulations arise from both variations in local composition and atomic positions. It is remarkable that the atomic planes affected by these variations are the $(111)_{RS}$ planes of the rock salt structure, i.e., the close packed layers as shown in Fig. 4 (long arrow) and Fig. 5.

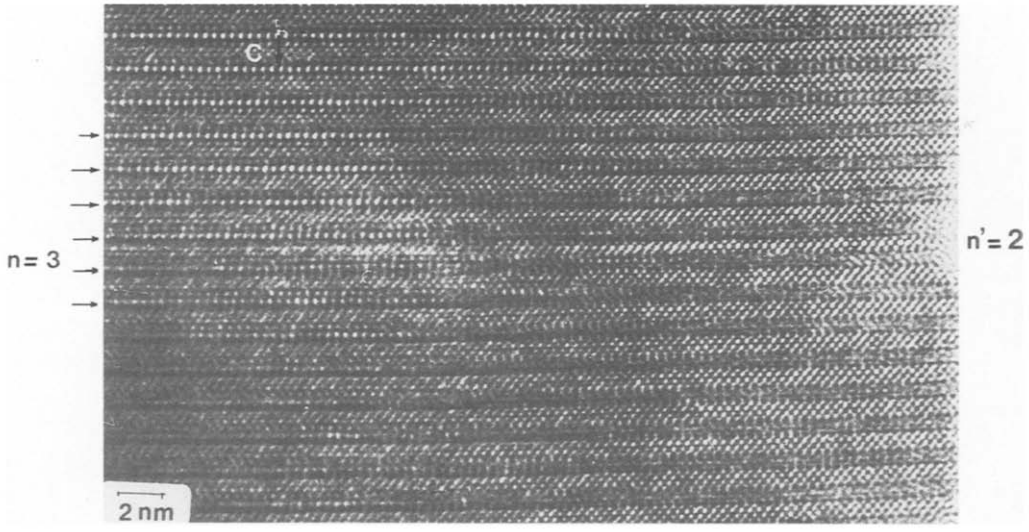

FIG. 11. Original defect showing the variation of the rock salt slice thickness in the bulk. In the left part of the image a periodicity corresponding to $n = 3$ is observed. On the right part, the $n' = 2$ defective member is easily observable. Note that this defect implies a local distortion of the crystal and a misorientation of the adjacent area.

(iii) In some parts of the crystals, modulations exhibiting a different wavelength are observed. They correspond to similar variations of the contrast in the $(111)_{RS}$ planes. An example is shown in the right part of Fig. 6, where the q value is close to $2 \times d_{100}$; for this focus value (≈ -775 Å) the white dots are correlated with the cation positions, and it clearly appears that, in the same way, the contrast variation is especially perceptible at the level of the rock salt layers (RS).

(iv) In other parts of the crystals, viewed along [100], strong undulations of the atomic planes are observed; the amplitude of the phenomenon is similar to that observed in the bismuth oxides. However, they differ by the direction $(100)_p$, the frequency (they are rare), and the nature of the atomic displacement; in the thallium compound the contrast is locally so disturbed that no correlation can be made between the image and the structure projection (Fig. 7).

(v) Along [001], modulations of the contrast are observed too, involving the existence of satellites on E.D. patterns. One example is given in Figs. 8a to 8c. The electron diffraction pattern corresponding to the selected area (Fig. 8a) exhibits satellites lying along [100]** and [010]*, as a result of the establishment of the modulation along the two equivalent directions of the tetragonal cell. The examination of these satellites

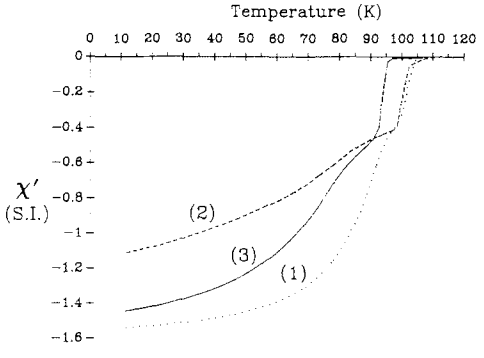

FIG. 12. ac susceptibilities $\chi'(T)$ of the Tl_2 (1), $Tl_{1.8}$ (2), and $Tl_{1.6}$ (3) as-synthesized samples.

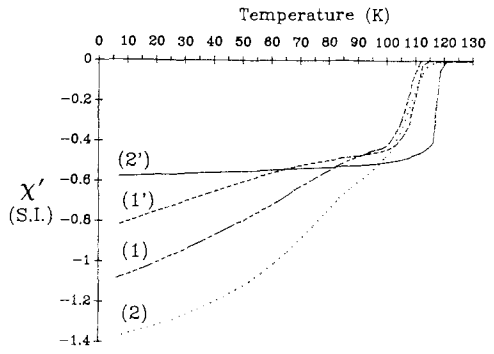

FIG. 13. ac susceptibilities $\chi'(T)$ of the Ar–H_2 270°C annealed samples. $Tl_{1.8}$: 30 min (1), 60 min (1′); $Tl_{1.6}$: 30 min (2), 90 min (2′).

shows that three main systems of nodes are observed, corresponding to $q \approx 4.3, 5.4$, and 12; it should be noted that for such areas, the reflections corresponding to $h + k \neq 2n$ are sometimes observed, attesting to a local loss of the symmetry. Figure 8b shows a zone where the modulation is established along a single direction but where the periodicity is variable along that direction. In the second zone of the crystal (Fig. 8c), the modulations set up along two orthogonal directions with two different periodicities ($5 \times d_{100}$ and $6 \times d_{010}$), leading to an apparent bidimensional modulation.

The fact that satellites, correlated with localized modulated domains in the crystals, are only observed in the thallium-deficient oxide suggests that they are directly correlated with the cation and anion deficiency. These modulations arise indeed in most of the crystals; however, their limited extents ($\ll 10\%$) show that they do not correspond to a systematical phenomenon but correspond only to local orderings of Tl, O, and vacancies.

Layer stacking. For the experimental conditions described above very few intergrowth defects are observed as well in the stoichiometric oxides as in the thallium-deficient oxides. They obey the general laws previously described (*22, 23*). Considering the general formula $(ACuO_{3-x})_m(AO)_n$, this thallium cuprate corresponds to $m = 2$ and $n = 3$. Only two defective perovskite layers $m' = 1$ and $m' = 3$ are observed, thus differing from the $m = 2$ matrix by $\Delta m = \pm 1$. A little more numerous are the defective rock salt slabs. They always corresponds to $n' = 2$ members; on average, only two or three events are observed in a crystal of several micrometers width. These defects are clearly observed on images where the $[AO]_\infty$ layers are highlighted: four rows of white dots corresponding to the sequence BaO–TlO–TlO–BaO are highlighted in the $n = 3$ members, whereas only three rows, corresponding to the sequence BaO–

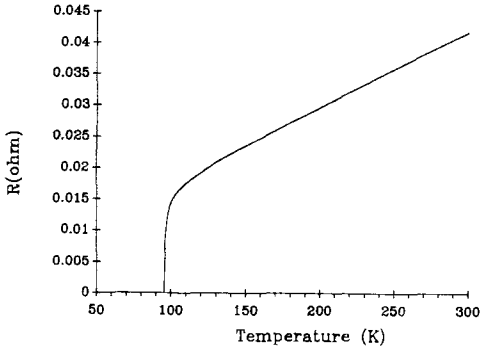

FIG. 14a. Electrical resistance versus temperature of the $Tl_{1.6}$ as-synthesized sample.

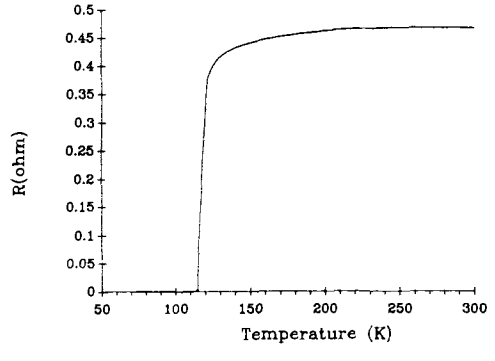

FIG. 14b. Electrical resistance versus temperature of the 90 min Ar–H_2 annealed $Tl_{1.6}$ sample.

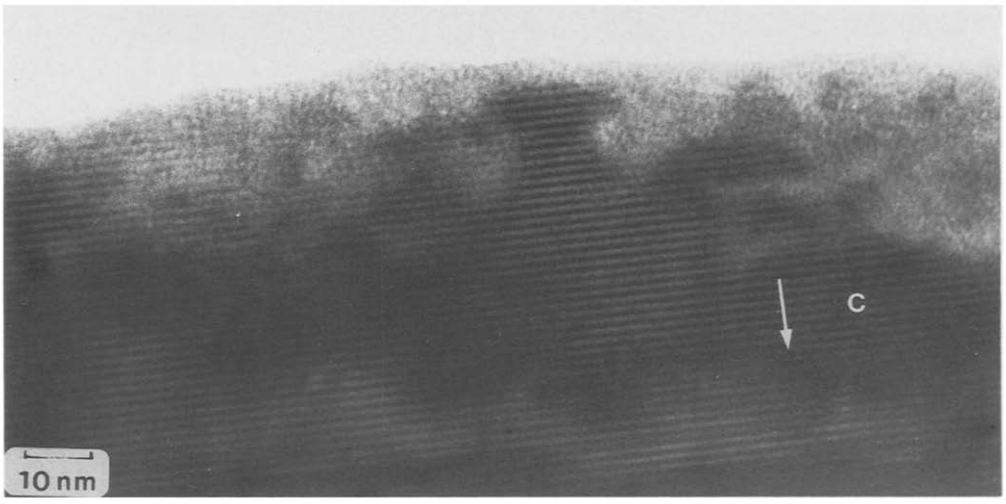

FIG. 15. [010] image showing the amorphization on the crystal edges of annealed samples.

TlO–BaO, are observed in the defective $n' = 2$ layer (Fig. 9). Lastly it should be noted that the $n' = 2$ members sometimes arise in locally ordered intergrowths with $n = 3$ members; the new sequence is always [$n = 3$, $n = 3$, $n = 2$] i.e., $n' = 2.66$ (Fig. 10).

One original type of defect, dealing with the layer stacking, has been observed (Fig. 11); it corresponds to the disappearance of a $[TlO]_\infty$ layer in the bulk. On the left part of the crystal, a regular periodicity of 1.4 nm is observed, corresponding to the half c value of an $n = 3$ member. On the right part, it appears clearly that an $n' = 2$ defective layer has replaced the $n = 3$ layer. It should be noted that this defect involves a local distortion of the crystal (bottom left part of the image).

Although the most frequent layer stacking defect corresponds to the existence of thallium monolayer, the rareness of the event allows one to rule out a mechanism of intergrowth for accomodating thallium deficiency. From this study, it appears that thallium atoms and vacancies can be considered as statistically distributed over the double TlO layers, but that this ion deficiency can result in local orderings which mainly arise in the $(111)_{RS}$ plane. In that way, satellites and modulations could be considered as indicative of cation and anion deficiency in the rock salt layers.

Influence of Thallium Nonstoichiometry upon Superconductivity

The 2212 T_c varies from 95 to 105 K depending on the synthesis conditions: temperature, pressure, heating time (*18, 14*). So all the samples (Tl_2 and deficients) were synthesized together in order to allow a comparison between the superconducting properties. The magnetization curve versus temperature for the $Tl_{1.6}$ sample (Fig. 12) is very close to that obtained for the Tl_2 sample in the same experimental conditions, i.e., for as synthesized materials prepared in a sealed tube with an oxygen pressure of about 8–10 bars and heated at 890°C for 8 hr. One observes a T_c of 96 K for $Tl_{1.6}$ to be compared to 104 K for Tl_2. This suggests that the hole carrier density does not vary dramatically from Tl_2 to $Tl_{1.6}$ oxide for simi-

lar experimental conditions, leading for $Tl_{1.6}$ to an increase of oxygen vacancies with respect to Tl_2. This view point is supported by the modulation of the structure, especially in the rock salt layers observed by HREM for $Tl_{1.6}$ sample; the latter may be due to the presence of oxygen vacancies, implying a displacive modulation of the atoms and also a modulated distribution of oxygen and vacancies over the anionic sites. The slight differences between T_c values can be explained by the difficulty to control the oxygen pressure with accurracy during the synthesis according to our experimental method.

The annealing effect of the thallium-deficient 2212 oxides, in an Ar/H_2 atmosphere, is very similar to that observed previously for stoichiometric $Tl_2Ba_2CaCu_2O_{8\pm\delta}$. Annealing of two $Tl_{1.8}$ and $Tl_{1.6}$ samples in an Ar/H_2 flow (90%–10%) at 270°C during 30 min allows their critical temperature to be increased up to 114 K, whereas a longer annealing of 90 min increases T_c to 120 K for the $Tl_{1.6}$ sample (Fig. 13). This improvement of T_c's by annealing under a reducing atmosphere confirms the predominant role of oxygen content in these phases with respect to thallium nonstoichiometry. As previously shown for Tl_2, the reducing atmosphere annealing tends to affect the grain boundaries; such an effect is clearly visible for the $Tl_{1.6}$ sample from susceptibility and resistivity curves. One indeed observes that at low temperature the χ' value decreases from -1.4 for the as-synthesized value to -0.6 for the 90 min-annealed sample (Fig. 13). In the same way, the resistivity curve of the as-synthesized sample (Fig. 14a) exhibits a metallic character above T_c (95 K), whereas the 90-min hydrogen-annealed $Tl_{1.6}$ sample shows no evidence of metallic behavior (Fig. 14b) above T_c, though its critical temperature has been increased to 120 K. These results are in perfect agreement with the electron microscopy observations, which show that the modulated structure inside the grains remains untouched for short annealing times, but that for long annealing times amorphization appears on the surface of the grains, explaining the grain boundary effects (Fig. 15).

Concluding Remarks

These results show that the thallium nonstoichiometry in the 2212-type structure does not affect greatly the superconducting properties of this material; they confirm that the oxygen nonstoichiometry remains the most important factor, since it allows the hole carrier density to be optimized in order to reach a critical temperature of 120 K, i.e., very close to that observed for the 2223-thallium cuprate. The modulated character of the rock salt layers in the thallium-deficient compounds does not seem to influence T_c's. Nevertheless, a detailed study of these layers should be interesting, if one admits that a homogeneous distribution of oxygen in the structure should allow the superconducting properties of these oxides to be improved.

References

1. A. Maignan, C. Michel, M. Hervieu, C. Martin, D. Groult, and B. Raveau, *Mod. Phys. Lett. B* **2**(5), 681 (1988).
2. R. M. Hazen, L. W. Finger, R. J. Angel, C. T. Prewitt, N. L. Ross, C. G. Hadidiacos, P. J. Heaney, D. R. Veblen, Z. Z. Sheng, A. El Ali, and A. M. Hermann, *Phys. Rev. Lett.* **60**(16), 1657 (1988).
3. B. Morosin, D. S. Ginley, E. L. Venturini, P. F. Hlava, R. J. Baughman, J. F. Kwak, and J. E. Schirber, *Physica C* **152,** 223 (1988).
4. A. Sulpice, B. Giordanengo, R. Tournier, M. Hervieu, A. Maignan, C. Martin, C. Michel, J. Provost, *Physica C* **156,** 243 (1988).
5. Z. Z. Sheng, L. Sheng, H. M. Su, and A. M. Hermann, *Appl. Phys. Lett.* **53**(26), 2686 (1988).
6. T. Kotani, T. Kaneko, H. Takei, and K. Tada, *JJAP* **28**(8) L1378 (1989).
7. K. K. Saini, C. P. Sharma, S. N. Ekbote, D. K. Suri, P. Asthana, K. C. Nagpal, Chanderkant, and S. Chandra, *Solid State Commun.* **74**(8), 789 (1990).

8. B. Morosin, R. J. Baughman, D. S. Ginley, J. E. Schirber, and E. L. Venturini, *Physica C* **165,** 115 (1990).
9. E. L. Venturini, B. Morosin, D. S. Ginley, J. F. Kawk, J. E. Schirber, R. J. Baughman, and R. A. Graham, *Mater. Res. Soc. Symp. Proc.* **156,** 239 (1989).
10. Y. Shimakawa, Y. Kubo, T. Manako, and H. Igarashi, *Phys. Rev. B.* **40**(16), 11400 (1989).
11. N. L. Wu and H. T. Chu, *Physica C* **167,** 267 (1990).
12. T. Zetterer, H. H. Otto, G. Lugert, and K. F. Renk, *Z. Phys. B: Condens. Matter* **73,** 321 (1988).
13. M. Greenblatt, S. Li. L. E. H. McHills, and K. V. Ramanujachary, *in* "Studies of High Temperature Superconductors" (A. V. Narlikar, Ed.), p. 143, Nova Science, New York (1990).
14. C. Martin, A. Maignan, J. Provost, C. Michel, M. Hervieu, R. Tournier, and B. Raveau, *Physica C* **168,** 8 (1990).
15. A. Maignan, C. Martin, M. Huve, J. Provost, M. Hervieu, C. Michel, and B. Raveau, *Physica C* **170,** 350 (1990).
16. K. V. Ramanujachary, S. Li, and M. Greenblatt, *Physica C* **165,** 377 (1990).
17. S. Nakajima, M. Kikuchi, Y. Syono, K. Nagase, T. Oku, N. Kobayashi, D. Shindo, and K. Hiraga, *Physica C* **170,** 443 (1990).
18. I. K. Gopalakrishnan, P. V. P. S. S. Sastry, H. Rajagopal, A. Sequeira, J. V. Yakhmi, and R. M. Iyer, *Physica C* **159,** 811 (1989).
19. B. Morosin, D. S. Ginley, E. L. Venturini, R. J. Baughman, and C. P. Tigges, *Physica C* **172,** 413 (1991).
20. M. A. Subramanian, J. C. Calabrese, C. C. Torardi, J. Gopalakrishnan, T. R. Askew, R. B. Flippen, K. J. Morrissey, U. Chowdhry, and A. W. Sleight, *Nature* **332,** 420 (1988).
21. D. B. Wiles and R. A. Young, *J. Appl. Crystallogr.* **14,** 149 (1981).
22. M. Hervieu, C. Martin, J. Provost, and B. Raveau, *J. Solid State Chem.* **76,** 419 (1988).
23. M. Hervieu, C. Michel, and B. Raveau, *J. Less-Common Metals* **150,** 59 (1989).
24. P. L. Gai, M. A. Subramanian, J. Gopalakrishnan, and E. D. Boyes, *Physica C* **159,** 801 (1989).
25. R. Moret, P. Gougeon, M. Potel, J. C. Levet, and H. Noel, *Physica C* **168,** 315 (1990).